This is to certify that the

thesis entitled

Tire models for the determination of vehicle structural loads

presented by

Robert Thomas Jane

has been accepted towards fulfillment
of the requirements for

Masters degree in Mechanical Engineering

James E Bernard
Major professor

Date 2/25/82

TIRE MODELS FOR THE DETERMINATION OF VEHICLE STRUCTURAL LOADS

By

Robert Thomas Jane

A THESIS

Submitted to
Michigan State University
in partial fulfillment of the requirements
for the degree of

MASTER OF SCIENCE

Department of Mechanical Engineering

1982

ABSTRACT

TIRE MODELS FOR THE DETERMINATION OF VEHICLE STRUCTURAL LOADS

By

Robert Thomas Jane

This thesis develops a tire model which estimates the magnitude and frequency of forces applied to the wheel spindle during low-speed tire/rough road interactions. A simple tire test to obtain input parameters for the model, and tests which validate the model are presented. The model is then used with a quarter car simulation to illustrate the utility of the model. Finally the limitations of the model for higher speed applications are examined.

ACKNOWLEDGEMENTS

I would like to thank my major professor and good friend, Dr. James E. Bernard, for his assistance and encouragement throughout my graduate studies.

I would also like to thank Jan Swift for her organizational assistance and typing of this dissertation.

I would also like to thank my parents, Clarence and Caroline Jane, for the support and guidance they have given me.

TABLE OF CONTENTS

LIST OF FIGURES

CHAPTER 1

Introduction

Directional response simulations of passenger cars have been in use since the 1950's. Since the trajectory of a vehicle is almost entirely dependent on the forces and moments applied to the vehicle from the road, the representation of the tire-road interface is of great importance. By and large, these directional response simulations have been limited to smooth road studies, and a variety of tire models have been developed for this purpose [4].

More recently, structural analysts have developed models which can reproduce modal properties of vehicles quite faithfully. These models are valuable in that the free vibrational modes of the automobile are indicators of structural performance. But an additional use of these models is the calculation of vibrational response, and or the stresses resulting from loading on the vehicle through the tires. This capability depends on additional information, the forces applied to the structure by the tires. This thesis was motivated by this need for tire forces generated during rough road vehicle simulations to be used as input to these complex vehicle models.

CHAPTER 2

Literature Survey

Two types of mathematical models of tires have been developed and presented in the literature. One type is the finite element model. This model is an excellent representation of a tire, but because of its complexity and high computing cost it is not used for tire-vehicle-system simulations. The remaining tire models are semi-empirical, they depend on the tire test data for their utility. Three of these models will be discussed here, the so-called point contact model, the fixed footprint model, and the adaptive footprint model.

Figure 1 presents the point contact model. This model has been extensively used in vehicle simulations to predict vertical forces for tires traversing smooth road surfaces. Davis, in Reference 7, claims that the point contact model is useful only if it is operated on a ground surface that exhibits the following characteristics:

(1) the road profile cannot have any step changes in elevation or slope.

(2) the elevation and slope of the road profile within the tire contact patch can be defined by a plane tangent to the ground at the "ground contact point".

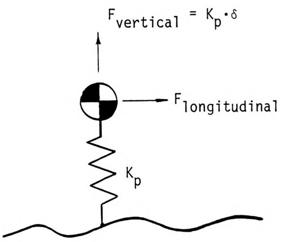

Figure 1. Point contact model.

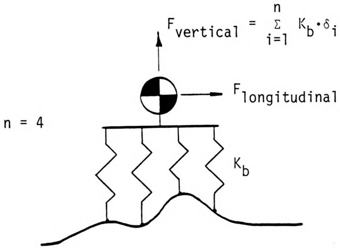

Figure 2. Fixed footprint model.

To overcome some of the shortcomings of the point contact model, the fixed footprint, or "brush" model was developed. In Reference 4 the fixed footprint model is discussed along with its use in vehicle simulations. As shown in Figure 2, the model consists of a number of parallel springs evenly spaced across the tire contact patch. The model has been used to successfully compute the vertical and longitudinal forces created by a tire slowly moving over an irregular road surface. But since the computation of longitudinal force depends on the local slope of the terrain, the fixed footprint model has its limitations. For example, the fixed footprint model predicts no longitudinal force upon encountering a step elevation change in terrain such as a curb.

A third formulation is the so-called adaptive footprint, or radial spring model. A diagram of the model is shown in Figure 3. The model assumes that:

(1) the tire is a thin disk that deforms only in the radial direction.

(2) the terrain is undeformable.

(3) the radial force-deflection relationship for the tire being modelled is known for a rigid planar surface.

Two procedures have been used to calculate forces for this model. A brief discussion of each follows:

The first method redefines the terrain contacting the tire model through the use of an "equivalent ground plane" that reflects the

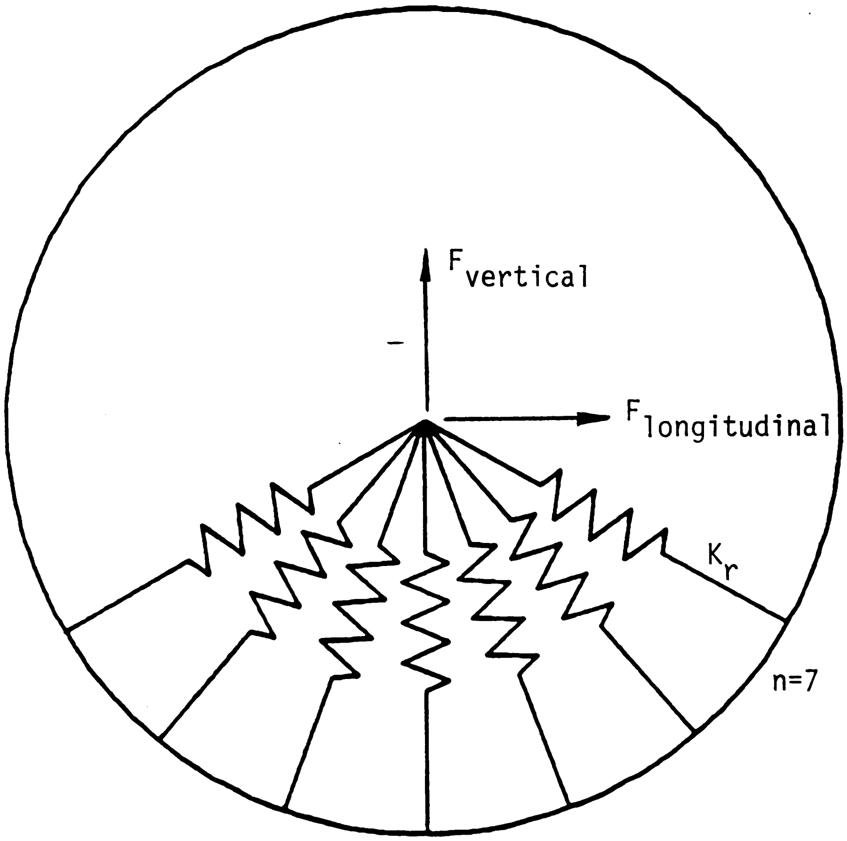

Figure 3. Radial spring model.

original elevation and slope of the terrain. Models of this type were presented by McHenry [6], and latter by Davis [7]. In McHenry's model, the tire is represented as a disk composed of nonlinear radial springs. The springs are spaced 4 degrees apart in the wheel disk, and have identical load-deflection characteristics that match the flat terrain properties of a nonlinear point contact model.

If a tire encounters irregular terrain, as in Figure 4, the tire model computes the forces as follows: At each point in time the individual radial spring deflections are computed. A vector summation of these deflections, is used in conjunction with the load-deflection properties of the radial springs to compute the resultant radial force vector, "equivalent ground contact point", and the "equivalent ground plane" of the tire. The resultant radial force vector is assumed to act through the "ground contact point", on a line through the wheel center.

It is important to note that the equivalent ground plane formulation assumes the net force vector acts through the wheel center. Since this assumption was not in agreement with our measurements, we were led to consider a second approach presented in [4], which does not require the resultant tire force to act through the wheel center. This model and some details of the supporting test program are presented in following sections of this thesis.

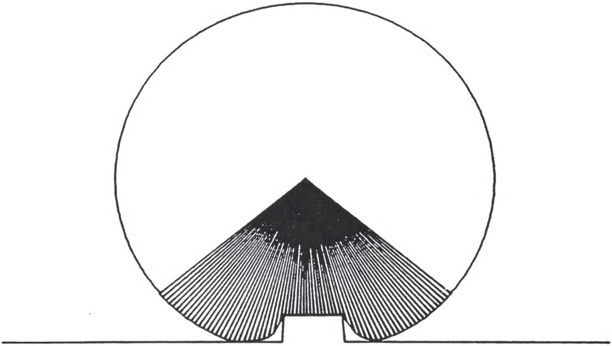

Figure 4. Radial spring model on 2" x 4" bump.

CHAPTER 3

The Model

Figure 3 is a schematic diagram of an adaptive footprint model. Algorithms used to compute forces at the tire/road interface for such a model have been presented in the literature by McHenry [6], Davis [7], and Captain [4]. The method employed here uses the radial spring deflections for force calculations, and neglects damping, as our goal is the simulation of low speed impacts. Higher speed impacts, where damping would be expected to be more important, will be discussed in Chapter 6.

The total force on the wheel hub can be expressed as the sum of all the forces created by the radial springs:

$$F = \sum_{i=1}^{n} \overline{d}f_i \qquad (3.1)$$

To calculate the individual force contributions from each spring, one might be led, as in [4], to use a linear relationship:

$$\overline{d}f_i = K_r * \overline{\delta}_i \qquad (3.2)$$

Where K_r represents a linear spring constant and $\overline{\delta}_i$ is the radial deflection of the ith spring. Since the tire model must support

the normal load, NS, of the tire at equilibrium, the following relation results:

$$NS = \sum_{i=1}^{n} K_r * \bar{\delta}_i \cdot \tilde{k} \qquad (3.3)$$

where $\tilde{k}$ is a unit vector in the vertical direction. This equation does not allow the value of K_r to be determined because the individual spring deflections, $\bar{\delta}_i$, are not known at the trim condition. Additional information is required to solve for K_r. Either the dynamic spring rate of the tire at equilibrium, or the contact patch length at equilibrium could be used. But if the dynamic spring rate is specified, the model's contact patch will not necessarily have the correct length, and if the contact patch length is specified, the resulting dynamic spring rate may be in error.

To deal with this situation, a nonlinear force-deformation relation was developed. This was done as follows: Consider a simple test in which the vertical tire force of a free rolling tire is measured as a function of wheel center height, as in Figure 5. The experimental data can be related to the sum of the vertical radial spring deflections, as shown in Figure 6, by simulating the same test using the radial spring model, thus yielding the summation of vertical spring deflections corresponding to the measured forces. Now vertical forces can be computed for any terrain by summing the vertical component of the radial spring deflections and finding the force from Figure 6.

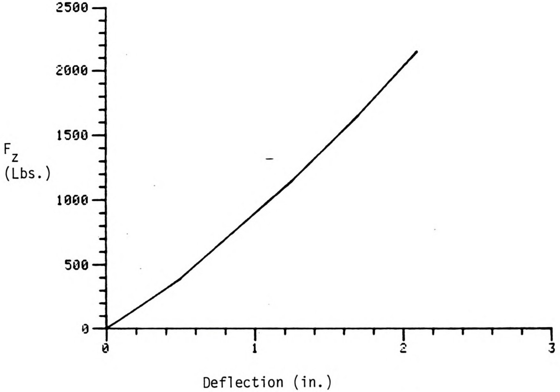

Figure 5. Force-deflection test data for a 14" Goodyear P185/75-R14 tire at 28 psi.

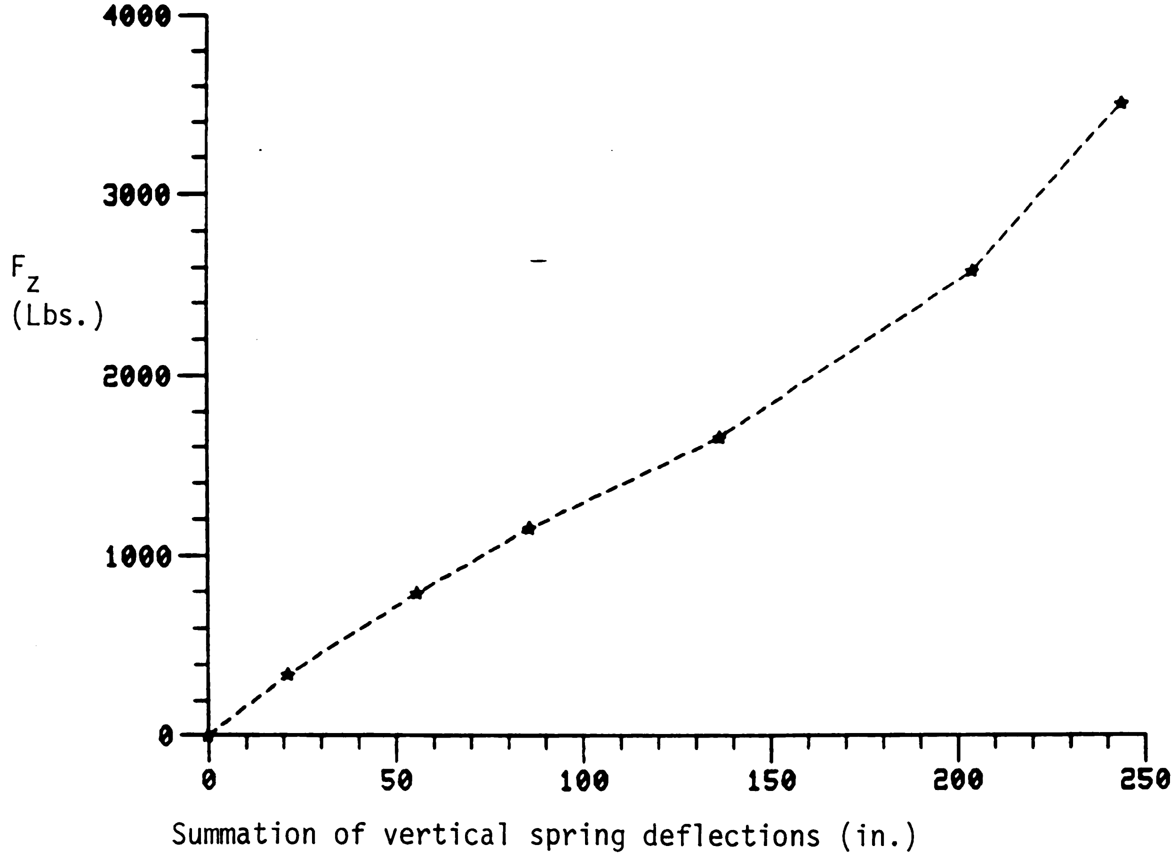

Figure 6. Table of vertical force as a function of vertical spring deflection.

Defining the vertical force versus total spring deflection in this way assures the correct dynamic spring rate as well as the proper contact patch length at the trim condition.

It is reasonable to assume that longitudinal forces can be computed using a similar algorithm. However, from the free rolling tire test results, it was found that a linear spring constant could be used to compute the longitudinal tire force:

$$F_x = \sum_{i=1}^{n} K_x * \bar{\delta}_i \cdot \tilde{i} \tag{3.4}$$

where $\tilde{i}$ is a unit vector in the longitudinal direction. It was found that setting the magnitude of K_x to ninety percent of K_r yielded excellent agreement between the test data and computed longitudinal forces.

An obvious question to be asked at this stage concerns the number of radial springs required to meet the objectives of the model. Its clear that the answer is not "one" - the point spring model has been shown to be inadequate for rough road simulations. On the other hand very large numbers of springs lead to increased computational expenses.

Related questions arise concerning enveloping. For example, if the deflection of each radial spring is computed by finding the intersection of the undeformed tire disk with the road profile, the awkward situation shown in Figure 7 may result. Computing forces in this manner assumes only radial deformation of each spring and ignores the forces and moments that can result if there is a stretching of the tire perimeter.

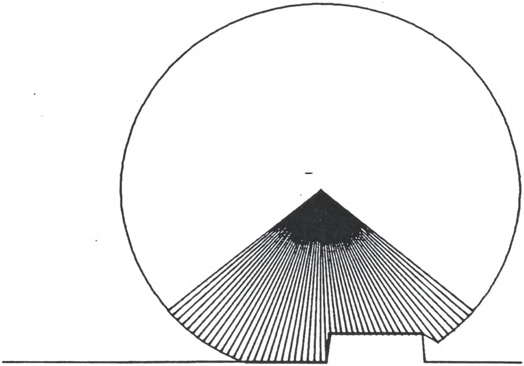

Figure 7. Radial spring model without shear force effects.

Since the stiffness of the tire perimeter precludes slope discontinuities such as those illustrated in Figure 7, the following algorithm was developed. Initially the deflection of each spring is computed based on the intersection of the undeformed tire disk with the road profile. Then a comparison is made between the vertical position of the endpoints of neighboring springs:

$$\delta Z_i = ZTIRE_i - ZTIRE_{i-1} \qquad i=2,\ n \tag{3.5}$$

where $ZTIRE_i$ represents the vertical position of spring i's endpoint with respect to the road. If the magnitude of δZ_i is greater than a given value, DELTA, then the endpoint position of springs close to spring i will be modified. The value of DELTA is determined by limiting the stretching of the tire circumference:

$$DELTA = R * d\theta \tag{3.6}$$

where R is the undeformed tire radius, and $d\theta$ is the angle between adjacent springs. This allows a maximum arc length of $\sqrt{2}$ * DELTA for each arc segment before the following algorithm is used to modify the tire profile. If a tire impacts a sharp bump, and the magnitude of δZ_i exceeds DELTA, then the M springs adjacent to spring i are to be modified, with M being computed by:

$$M = \frac{|\delta Z_i|}{DELTA} \tag{3.7}$$

The spring endpoints being modified are always lower than spring i. For example, if a tire is going up a bump, then the springs before spring i are modified using the following equation:

$$ZTIRE_{\ell} = ZTIRE_{\ell} + \frac{\delta Z_i}{\frac{5}{4}\ell * 1.05}(\ell-1)^2 \qquad \ell=1,\ M \qquad (3.8)$$

where ℓ is a counter that moves to the left or right of spring i.

Figure 8 illustrates the resulting smoothing created when a tire encounters a 2" by 6" bump. Note the greater movement of the springs close to the object with a decreasing effect on the springs located away from the obstruction. In this example, δZ_i becomes greater than DELTA when i=21, or between the twenty and twenty-first springs. By computing M as previously discussed, it is found that the seventeen springs before spring 21 must be modified.

Using this enveloping algorithm, with 200 radial springs evenly spaced across the 2 radian arc of the tire model led to realistic tire profiles. Computing the tire profile with this intuitively based approach to account for tread shear force led to very good correlation with test data. This will be discussed in the next section.

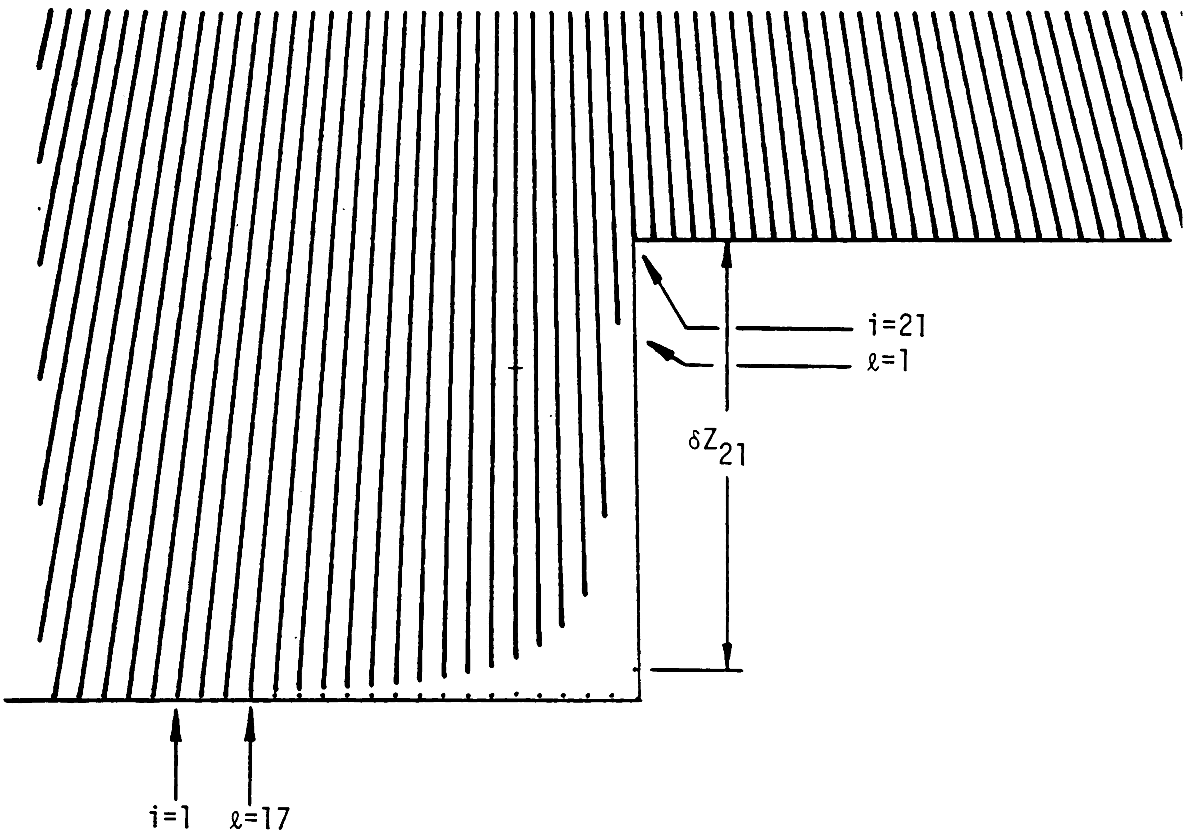

Figure 8. Closeup of tire profile using shear force algorithm during a bump/tire impact.

CHAPTER 4

Model Validation

To validate the modified radial spring model, rolling tire tests were performed at the Highway Safety Research Institute in Ann Arbor, Michigan, using a flat bed tire testing machine [6]. The flat bed test machine is instrumented to measure all of the forces and moments created by a tire rolling along the test bed. To simulate rough road conditions, various sized wooden blocks were placed on the test bed and allowed to move under the tire while the wheel spindle height was held constant. The tests were made using a bed speed of three ft/sec, the standard speed of the test machine.

To gather parameters for the modified radial spring model, the vertical force vs. deflection was measured for a Goodyear P185/75-14 radial tire, inflated to 28 psi. The input data was gathered by varying the wheel spindle height, and measuring the resulting vertical force as the tire rolled along the flat bed of the test machine. Figure 5 presents this data.

To validate the modified radial spring model output for rough road simulations, the flat bed test machine was used to gather test data. Road disturbances were provided by wooden blocks placed on the bed of the test machine. The dimensions of the blocks used were two inches high by six inches long, and one inch high by six inches long. In both cases the wooden blocks were of sufficient width to eliminate any lateral force generation. Both vertical and longitudinal tire forces were measured using a strip chart recorder to record the forces.

Figure 9 presents the measured test data and the computed model output for vertical force versus longitudinal position as the tire encounters each of the wooden blocks. The vertical force output was expected to be symmetric since the bump was symmetric and because the wheel spindle was held at a fixed height. The Figure shows a static normal load of 800 pounds was present in the tire, and the peak vertical force was generated as the wheel spindle passed over the center of the bump, occuring at x=15.5 inches. The symmetric plots of the model output and the tire test results are in close agreement.

The results of the tire testing program also suggested that a linear spring constant K_x would be sufficient to compute the longitudinal forces for the radial spring model. A comparison of longitudinal tire force calculated using this linear spring are presented in Figure 10. The figure incidates that the free rolling test data and simulation produce symmetric, very similar results. As the leading edge of the tire first impacts the bump, a negative or rearward force is produced. Then as the wheel center passes directly over the bump, the longitudinal force passes through zero and becomes positive, or forward, as the tire begins to move down off the bump.

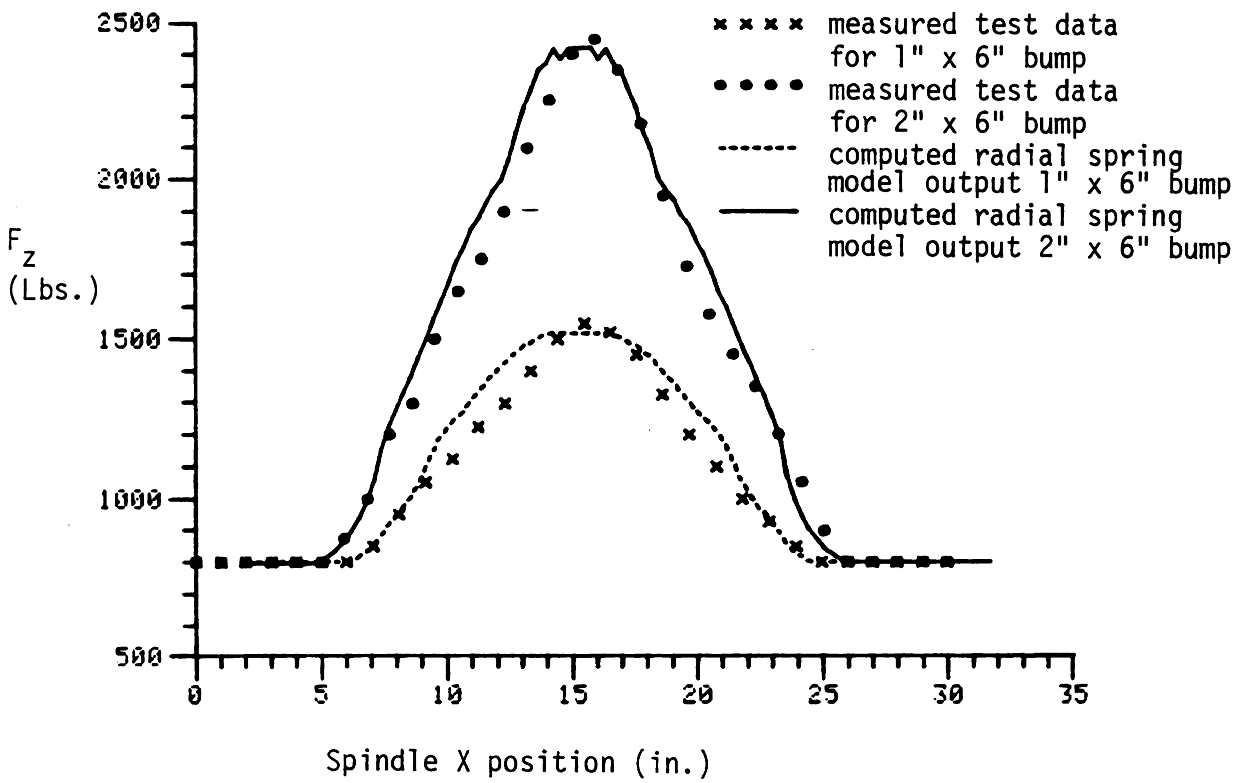

Figure 9. Measured and computed vertical tire forces for a 14" Goodyear P185/75-R14 tire at 28 psi.

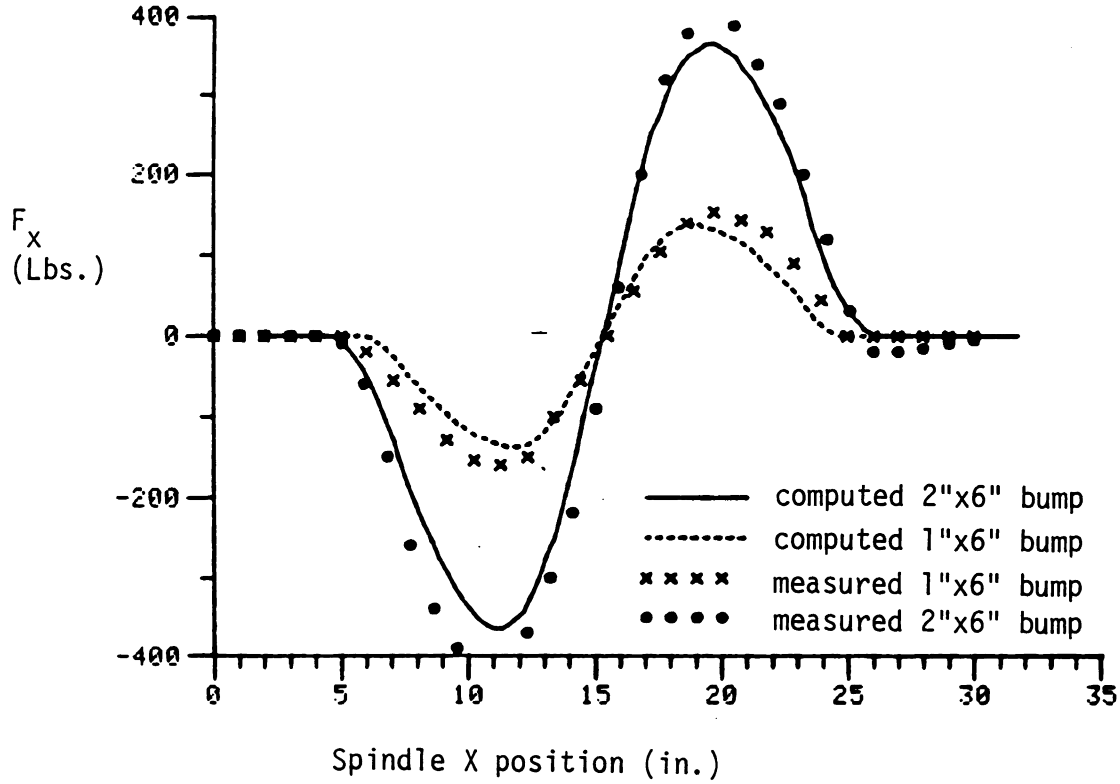

Figure 10. Measured and computed longitudinal tire forces for a 14" Goodyear P185/75-R14 tire at 28 psi.

CHAPTER 5

Vehicle Simulation

To illustrate the utility of the modified radial spring model, a so-called quarter car model simulation was implemented. Figure 11 presents a schematic diagram of the model. The vehicle model has two degrees of freedom, the vertical position of the wheel, the unsprung mass, and the vertical position of the car body, the sprung mass. These two quantities are represented by Zw and Zb respectively.

A variety of tire models could be used to compute the forces at the tire/road interface. For purposes of comparison here, two tire models were used, a simple point contact model, and the modified radial spring model. The parameters input to both of these tire models are representative of 14" radial car tires, and are presented in Table 5.1. The vehicle parameters are presented in Table 5.2, indicating a simple approximation for a 3200 pound car.

TABLE 5.1 Tire Parameters

Radial spring model..................Figure 5

Point contact model..................K_p=1000 Lb/in.

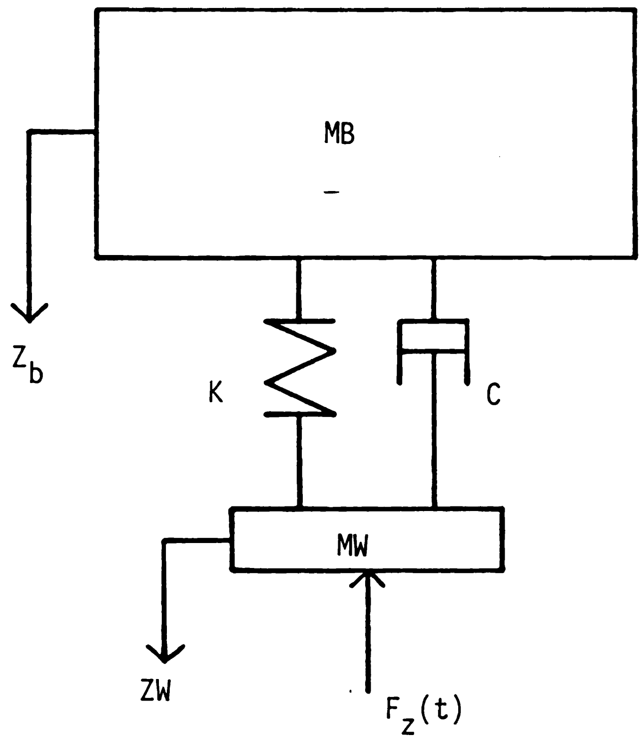

Figure 11. Quarter car model.

where K_p is a linear spring constant used to compute vertical force for the point model.

TABLE 5.2 Vehicle Parameters

K (suspension spring stiffness)...............100 lb/in

C (suspension damping coefficient)............2.2 lb-sec/in

MB X g (weight sprung mass)...................700 lbs

MW X g (weight unsprung mass).................100 lbs

To study the effect of the tire model on transient response, a low speed impact with a 2" high by 6" long bump was simulated. Figures 12 through 14 present the computed output for the quarter car model. Figure 12 presents the resultant vertical force created at the tire/road interface. The Figure indicates that the vertical force spike of the point model begins when the wheel center is directly over the leading edge of the road obstruction, and ends as the wheel center passes the end of the obstruction. The force which occurs immediately after the center line of the tire reaches the bump, is the product of the point spring rate and the height of the bump. The force output of the radial spring model has a more realistic time history with the vertical force building up before the wheel center reaches the bump, and decaying after the wheel center has passed over the end of the obstruction.

The resulting rigid body motions are shown in Figures 13 and 14. The Figures indiciate that the higher frequency content

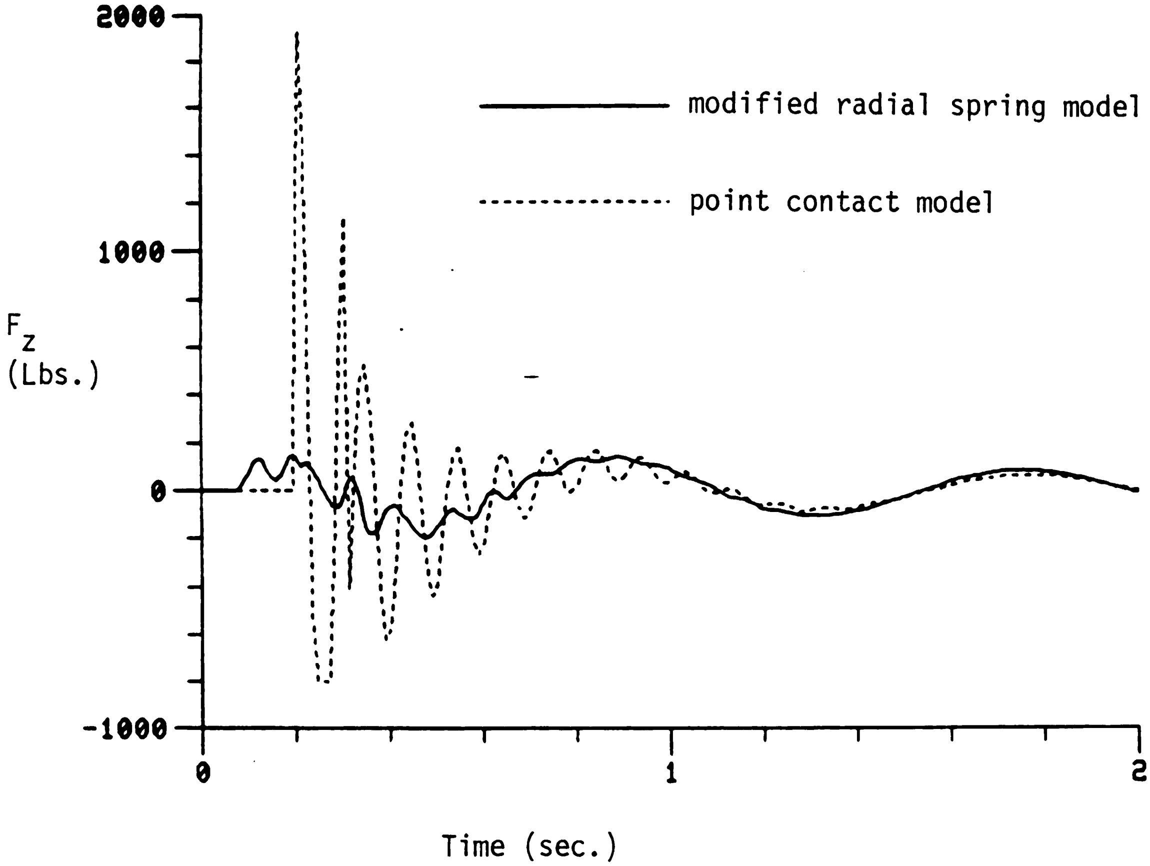

Figure 12. Vertical tire forces, impact speed 3 (feet/sec.).

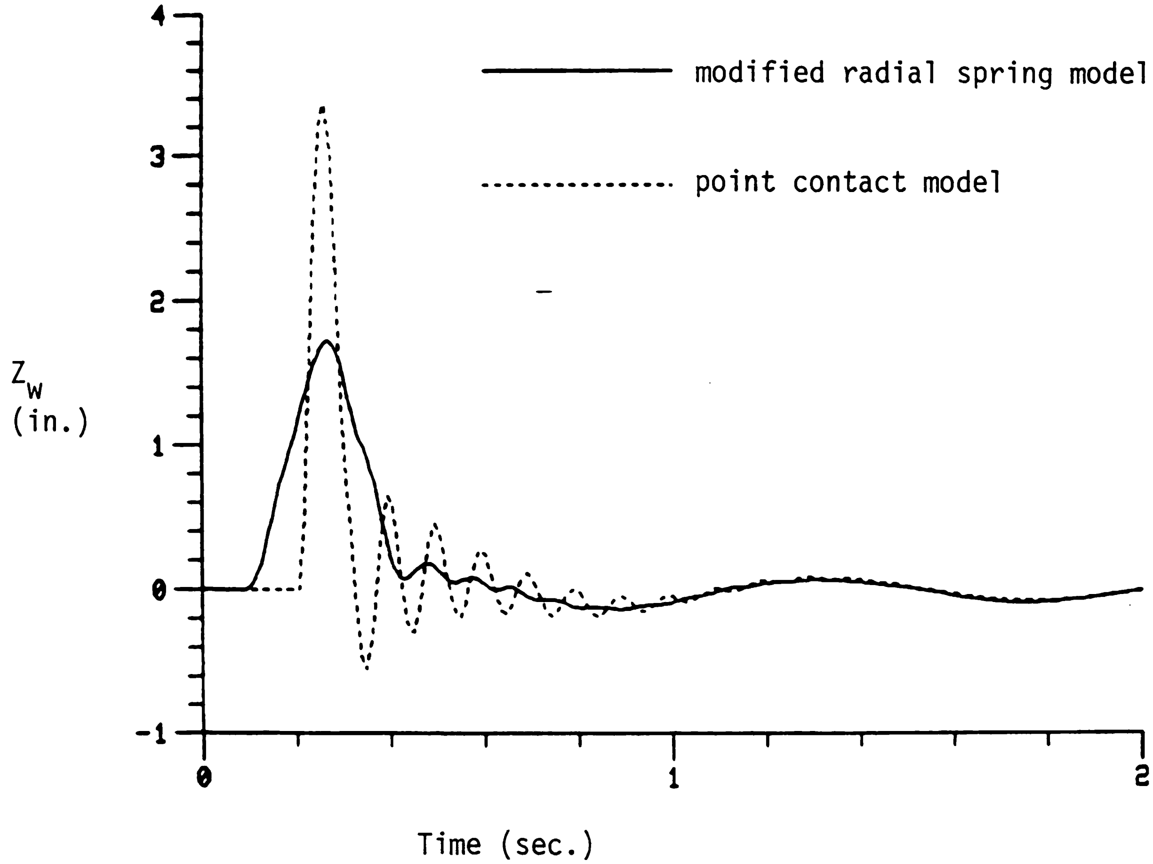

Figure 13. Wheel spindle displacement, impact speed 3 (feet/sec.).

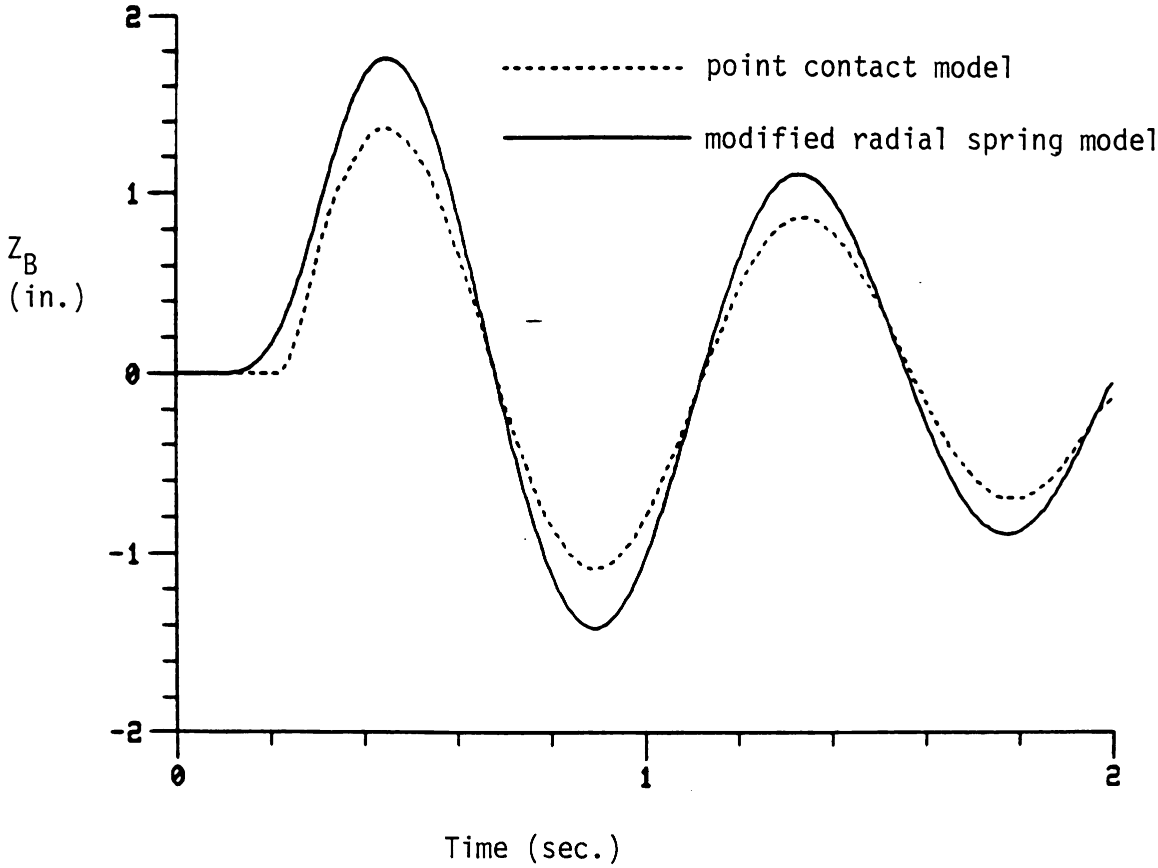

Figure 14. Car body displacement, impact speed 3 feet/sec.

of the point model leads to enhanced excitation of the wheel hop mode of vibration, and less excitation of the car body. The more realistic force-time history created by the radial spring model leads to smaller wheel displacement; and larger car body motion.

All of the work so far presented has been of low speed testing and simulations. The next section is concerned with higher speed impacts.

CHAPTER 6

Spin Constraint

In the free rolling tire tests presented in Figures 9 and 10, the tire was unconstrained by any moments applied about the spin axis by the tire testing apparatus. The angular spin rate, ω, was able to vary as the tire traveled over the test block. In particular, the longitudinal velocity of the wheel center relative to the ground was held constant, and the spin rate, ω, increased as spindle-to-ground distance is decreased, thus avoiding longitudinal stretching of the tire contact patch. This section will consider similar tests in which the wheel spin rate was held constant.

Figure 15 presents the longitudinal force test data for a 14" radial passenger car tire impacting the 2" x 6" block with spin rate held constant, and the free rolling test data of the same impact. The symmetric plot of the free rolling tire contrasts the biased forces measured when the tire was not permitted to spin up as it encountered the wooden block. As the rolling radius of the tire is shortened by the tire/block interaction, the constant angular velocity of the tire, ω, maintained by the flat bed test machine servo drive becomes smaller than the spin rate required for no longitudinal slip. As a result, the force bias caused by this longitudinal slip is in the negative or rearward sense. The

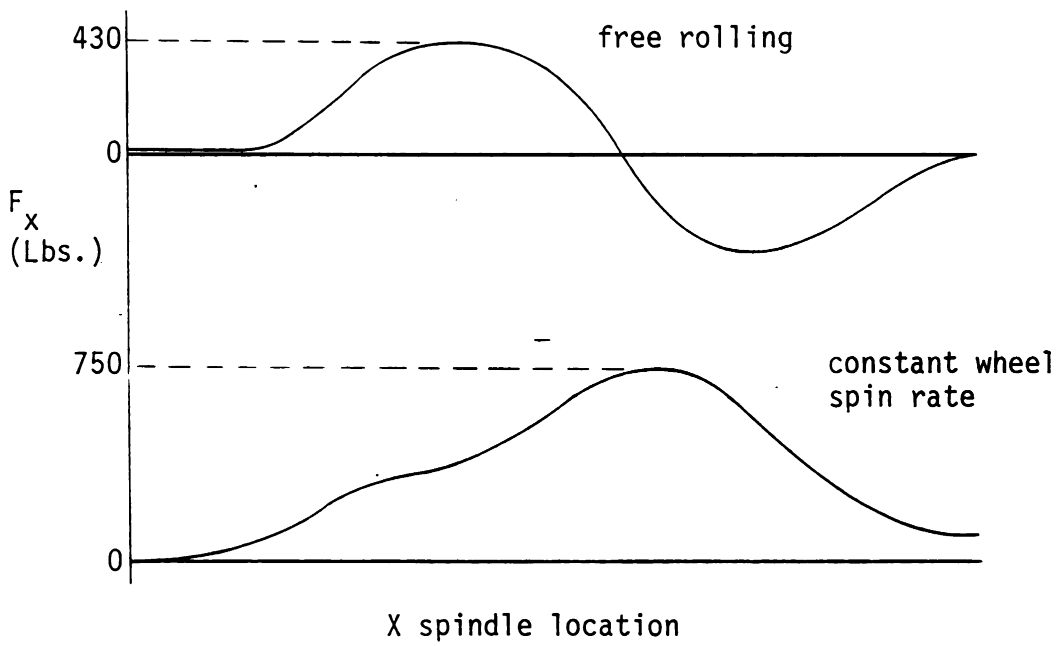

Figure 15. Longitudinal force biasing. Test data from a 14" Goodyear P185/75-R14 tire at 28 psi.

vertical tire force, on the other hand, did not show substantial changes when the spin rate of the tire was constrained to remain constant during tire testing.

A simple simulation was used to aid in understanding these results. In this simulation longitudinal brake force was assumed to be a function of the longitudinal tire slip, S, where:

$$S = 1 - R\omega/U \qquad (6.1)$$

R is the average length of the radial springs in the contact patch; ω is the wheel spin rate, and U is the longitudinal velocity of the wheel spindle.

Using a simple μ-slip curve, shown in Figure 16, to compute the brake forces caused by longitudinal tire slip, a simulation of the tire impacting the 2" x 6" bump at various speeds was implemented. The results of this simulation are presented in Figure 17.

The simulation of the low speed impact indicated a symmetric longitudinal force as the tire crossed the bump, in good correlation with the free rolling tests. But as the speed, U, is increased, the simulation predicts a force bias similar to the one created during the constrained wheel spin testing. This non-symmetric force output is expected because as the longitudinal velocity is increased, the tire/wheel assembly does not have sufficient time to spin up while the tire is in contact with the test block. This inability to spin up creates a deformation of the tire contact patch, and therefore large brake forces due to longitudinal slip of the

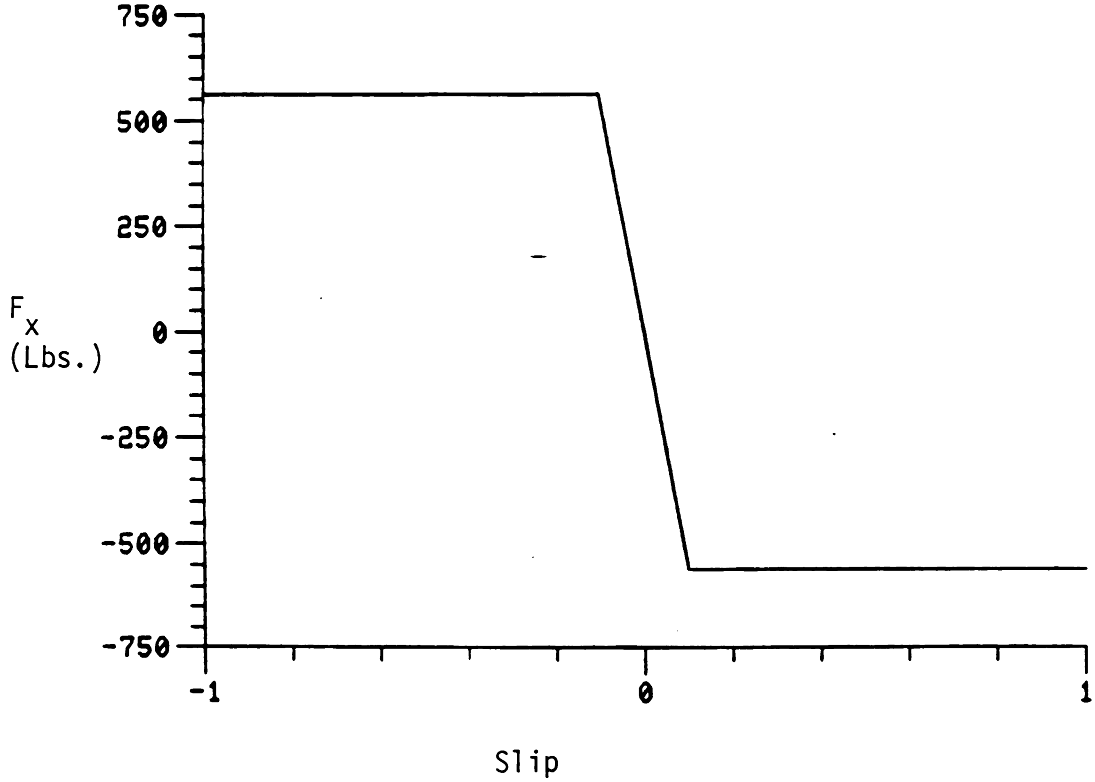

Figure 16. Longitudinal tire force due to tire slip.

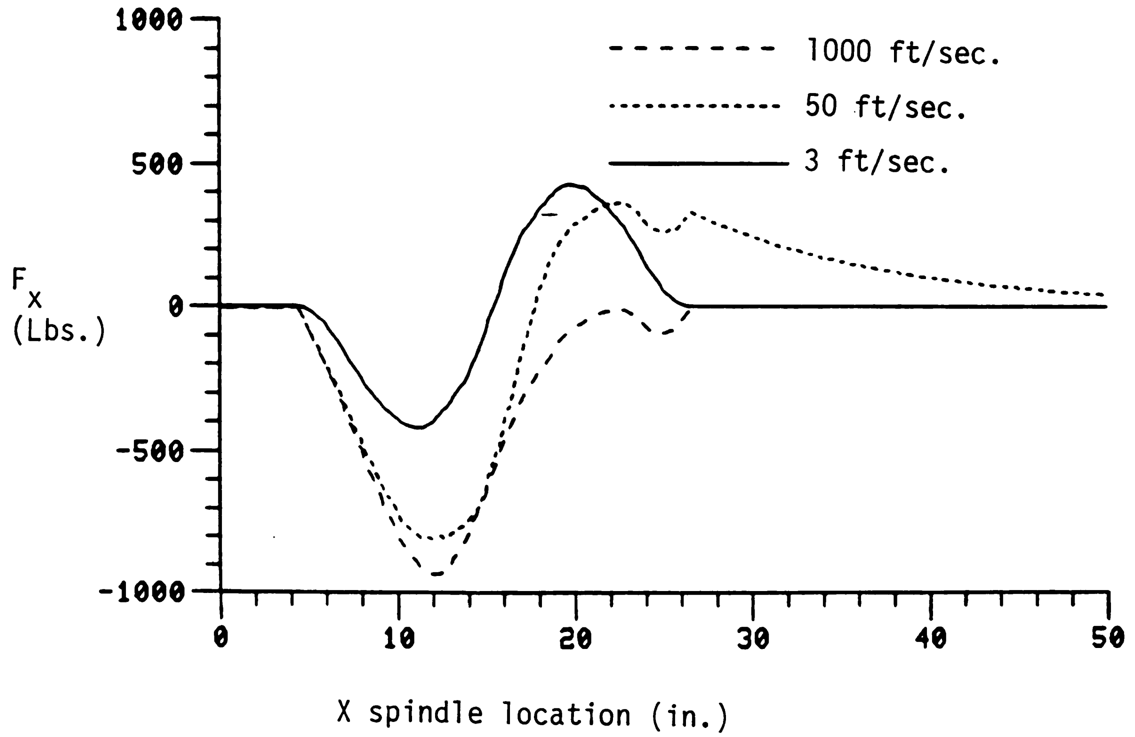

Figure 17. Effect of vehicle speed on longitudinal tire force.

tire. The highest velocity, which effectively holds the tire spin rate constant during the tire/bump impact, leads to a result very similar to the results measured while testing with the wheel spin rate constrained.

The simulation predicts little longitudinal force biasing for tire/bump impacts with longitudinal velocity less than ten feet per second.

CHAPTER 7

Conclusions

The modified radial spring model yields accurate vertical and longitudinal tire forces created during tire/rough road interaction at low speeds. The model requires a minimum of input data, which can be gathered by measuring the vertical force-deformation relationship of the tire.

The longitudinal forces generated by the model at high speeds are expected to be inaccurate due to the significant force biasing created by longitudinal tire slip. Further work should include high speed testing to confirm the effects of wheel spin rate on tire forces.

LIST OF REFERENCES

LIST OF REFERENCES

1. Segel, L., "Theoretical Prediction and Experimental Substantiation of the Response of the Automobile to Steering Control," Proc. Auto. Div., The Instn. Mech. Engrs., No. 7, p. 310 (1956-1957).

2. Ellis, J., "The Dynamics of Vehicles During Braking," Symp. Cont. of Vehicles, Instn. Mech. Engrs., Proc., pp. 20-29 (1963).

3. Bernard, J.E., Segel, L., and Wild, R.E., "Tire Shear Force Generation During Combined Steering and Braking Maneuvers", SAE paper No. 770852.

4. Captain, K.M., Boghani, A.B., and Wormley, D.M., "Analytical Tire Models for Dynamic Vehicle Simulation", Vehicle System Dynamics 8 (1979) pp. 1-32.

5. Rasmussen, R.E., and Cortese, A.D., "The Dynamic Spring Rate of Rolling Tires", SAE paper No. 680408.

6. McHenry, R. et al., "Vehicle Dynamics in Single Vehicle Accidents", Cornel Aeronautical Laboratories, Report No. VJ-2251-V-3, December, 1968.

7. Davis, D.C., "A Radial Spring Terrain-Enveloping Tire Model", Vehicle System Dynamics 3 (1974), pp. 55-69.